Investigating the Role of Shrub Height and Topography in Snow Accumulation on Low-Arctic Tundra using UAV-Borne Lidar

Maxim Lamare, Florent Domine, Jesús Revuelto, Maude Pelletier, Laurent Arnaud, Ghislain Picard

Investigating the Role of Shrub Height and Topography in Snow Accumulation on Low-Arctic Tundra using UAV-Borne Lidar

MAXIM LAMARE,[a,b] FLORENT DOMINE,[c,d] JESÚS REVUELTO,[e] MAUDE PELLETIER,[f] LAURENT ARNAUD,[b] AND GHISLAIN PICARD[b]

[a] *Centre d'Études de la Neige, Université Grenoble-Alpes, Université de Toulouse, Météo-France, CNRS, CNRM, Grenoble, France*
[b] *Institut des Géosciences de l'Environnement, UMR 5001, Université Grenoble Alpes, CNRS, Grenoble, France*
[c] *Takuvik Joint International Laboratory, Université Laval (Canada) and CNRS-INSU (France), Université Laval, Quebec, Quebec, Canada*
[d] *Department of Chemistry and Centre for Northern Studies, Université Laval, Quebec, Quebec, Canada*
[e] *Instituto Pirenaico de Ecología, Consejo Superior de Investigaciones Científicas, Zaragoza, Spain*
[f] *MVT GEO-SOLUTIONS, Quebec, Quebec, Canada*

(Manuscript received 27 April 2022, in final form 13 February 2023, accepted 16 February 2023)

ABSTRACT: Expanding shrubs in the Arctic trap blowing snow, increasing snow height and accelerating permafrost warming. Topography also affects snow height as snow accumulates in hollows. The respective roles of topography and erect vegetation in snow accumulation were investigated using a UAV-borne lidar at two nearby contrasted sites in northern Quebec, Canada. The North site featured tall vegetation up to 2.5 m high, moderate snow height, and smooth topography. The South site featured lower vegetation, greater snow height, and rougher topography. There was little correlation between topography and vegetation height at both sites. Vegetation lower than snow height had very little effect on snow height. When vegetation protruded above the snow, snow height was well correlated with vegetation height. The topographic position index (TPI) was well correlated with snow height when it was not masked by the effect of protruding vegetation. The North site with taller vegetation therefore showed a good correlation between vegetation height and snow height, $R^2 = 0.37$, versus $R^2 = 0.04$ at the South site. Regarding topography, the reverse was observed between TPI and snow height, with $R^2 = 0.29$ at the North site and $R^2 = 0.67$ at the South site. The combination of vegetation height and TPI improved the prediction of snow height at the North site ($R^2 = 0.59$) but not at the South site because vegetation height has little influence there. Vegetation was therefore the main factor determining snow height when it protruded above the snow. When it did not protrude, snow height was mostly determined by topography.

SIGNIFICANCE STATEMENT: Wind-induced snow drifting is a major snow redistribution process in the Arctic. Shrubs trap drifting snow, and drifting snow accumulates in hollows. Determining the respective roles of both these processes in snow accumulation is required to predict permafrost temperature and its emission of greenhouse gases, because thicker snow limits permafrost winter cooling. Using a UAV-borne lidar, we have determined snow height distribution over two contrasted sites in the Canadian low Arctic, with varied vegetation height and topography. When snow height exceeds vegetation height, topography is a good predictor of snow height, with negligible effect of buried vegetation. When vegetation protrudes above the snow, combining both topography and vegetation height is required for a good prediction of snow height.

KEYWORDS: Complex terrain; Snow; Vegetation; Snow cover; Lidars/Lidar observations

1. Introduction

In northern regions, the snow cover insulates the ground from the winter cold air and therefore plays a key role in the permafrost thermal regime (Zhang 2005). With global warming, shrubs are expanding on Arctic tundra (Ju and Masek 2016; Tremblay et al. 2012) and this has been observed to lead to increases in snow height in some cases (Busseau et al. 2017; Sturm et al. 2001). Here, we use the term "snow height" rather than the more common "snow depth" because we take the ground surface as the origin, for consistency with vegetation height. Since the thermal insulance of the snowpack increases with height (Sturm et al. 2005b), and since furthermore snow in shrubs can be more insulating because of a lower thermal conductivity (Domine et al. 2016; Sturm et al. 2001), shrub expansion and growth on Arctic tundra may reduce permafrost winter cooling and therefore accelerate permafrost warming. Such warming leads to active layer thickening (Boike et al. 2018) and to geomorphological changes such as active layer detachment slides (Costard et al. 2021; Mithan et al. 2021) and the formation of thermokarst ponds (Farquharson et al. 2019). These processes

Denotes content that is immediately available upon publication as open access.

Supplemental information related to this paper is available at the Journals Online website: https://doi.org/10.1175/JHM-D-22-0067.s1.

Corresponding author: Florent Domine, florent.domine@gmail.com

DOI: 10.1175/JHM-D-22-0067.1

lead to the thawing of some of the organic matter stored in permafrost, allowing their microbial degradation, which results in emissions of CO_2 and CH_4, positively feeding back on climate warming (McGuire et al. 2018).

How shrub expansion and growth impacts snow height is therefore an important aspect in the thermal evolution of permafrost and climate. This process is not simple because many factors are involved. Conventional wisdom on the topic is that since shrubs decrease wind speed within or around them, they facilitate snow trapping within their structure and downwind of it and therefore higher vegetation leads to greater snow accumulation (Duguay and Bernier 2012; Essery and Pomeroy 2004; Sturm et al. 2001). However, shrubs may grow preferentially in hollows where the soil is more humid and where snow preferentially accumulates (Gagnon et al. 2019; Marsh et al. 2020; Pelletier et al. 2019; Revuelto et al. 2020; Sturm et al. 2001; Winstral and Marks 2002) so that the greater snow height in shrubs may partly or wholly be ascribed to topography. The efficacy of snow accumulation in shrubs may also be highly variable and in particular may depend on the snow supply. Essery and Pomeroy (2004) modeled that beyond a certain height, taller shrubs did not increase snow accumulation because of limitations in snow supply. Furthermore, shrubs absorb solar radiation and emit longwave radiation, sometimes leading to snowmelt and a decrease in snow height. This is frequent in fall and spring (Barrere et al. 2018; Busseau et al. 2017; Sturm et al. 2005a) but may also happen during winter warm spells.

Snow–shrub interactions are complex and multifaceted, so it may not be possible to simply sum up the impact of shrubs on snow height by invoking a wind reduction–snow accumulation effect. Relevant observations at the microscale (1–10 m), adequate for detailed process understanding are few in the Arctic (Sturm et al. 2001). Modeling studies have investigated the impact of topography and/or vegetation on snow redistribution by wind (Essery and Pomeroy 2004; Marsh et al. 2020; Pomeroy et al. 1993; Vionnet et al. 2017; Winstral and Marks 2002; Winstral et al. 2013). Those studies had mainly hydrological objectives and focused on snow redistribution at a large scale. Field validation consisted mostly in global snow mass budgets. They concluded that large snow accumulations in the absence of vegetation were indeed largely dictated by topography (Winstral and Marks 2002) and that taller shrubs or stubble usually led to greater snow accumulation than shorter vegetation (Essery and Pomeroy 2004; Pomeroy et al. 1993) provided that there was a sufficient snow supply.

Snow height mapping at fine spatial resolution by airborne investigations have until fairly recently been unable to investigate the effect of shrubs on snow height. Photogrammetry (structure from motion) has been used for this purpose on open environments with accuracies better than 5 cm (Harder et al. 2016; Revuelto et al. 2021). However, in the presence of erect vegetation such as shrubs or trees, photogrammetry only senses the top of the vegetation rather than the actual ground (De Michele et al. 2016; Fernandes et al. 2018; Harder et al. 2020) so that snow height cannot be determined by comparing summer and winter elevation maps.

Lidar studies have been more successful because the lidar beam is reflected by both the vegetation and the ground if the leaf density remains moderate. This allows the determination of the ground level below vegetation in the snow-free season, so that snow height can subsequently be determined by winter measurements (Deems et al. 2013; Harder et al. 2020). This has been used successfully to map snow height in forests (Koutantou et al. 2022; Mazzotti et al. 2019; Schneider et al. 2020; Uhlmann et al. 2018). However, to the best of our knowledge, snow height distribution on shrub tundra has not been investigated by lidar, other than for methodological objectives (Currier et al. 2019; Painter et al. 2016; Tinkham et al. 2014). Shrubs and forest affect snow drift differently because trees are always higher than snow and prevent snow erosion over large expanses. Snow in forest thus remains of low density over the whole forested areas (Sturm et al. 1995). Shrub tundra on the contrary is less homogeneous with numerous shrubless patches (Belke-Brea et al. 2020; Domine et al. 2022; Lemay et al. 2018; Sturm et al. 2001) so that shrubs are not expected to prevent snow drifting as efficiently as trees.

The detailed understanding of the combined effects of topographic and shrub vegetation on snow accumulation in windy conditions requires data at very fine spatial resolution, of the order of vegetation height. Such detailed processes have not been investigated by modeling, and no detailed field measurements are available. As recently stated by Marsh et al. (2020), topography and vegetation have different interactions with wind: "The inclusion of vegetation interactions on the wind field is a major source of uncertainty, and properly capturing the wind flow through protruding vegetation would require even greater detail in the wind model and is an open research question." Investigating the detailed impact of topographic and vegetation features on snow redistribution, and comparing the effects of both types of features is therefore timely and necessary for improving our understanding of wind–snow–vegetation–topography interactions.

To contribute to these questions, we have measured snow height at the cm scale over low-Arctic tundra comprised of a variety of vegetation covers including lichen, low shrubs, tall shrubs, and stunted trees, using lidar scanning by an unmanned aerial vehicle (UAV). The selected location is Tasiapik valley near Umiujaq, northern Quebec, Canada, which features varied topography with flat areas, slopes, gullies, and permafrost mounds (lithalsas) (Beck et al. 2015; Fortier et al. 2020; Provencher-Nolet et al. 2014). We obtained data near peak snow height so that the possible impacts of fall and spring melt episodes were not explored. The main questions addressed here are:

(i) Does vegetation height impact snow height?
(ii) Does topography impact snow height?
(iii) How do topography and vegetation height interact in determining snow height?

2. Methods

a. Site

We performed high-resolution snow height measurements over two ~0.5-km-long areas (hereafter North site and South site) near the community of Umiujaq, in Tasiapik Valley (Fig. 1).

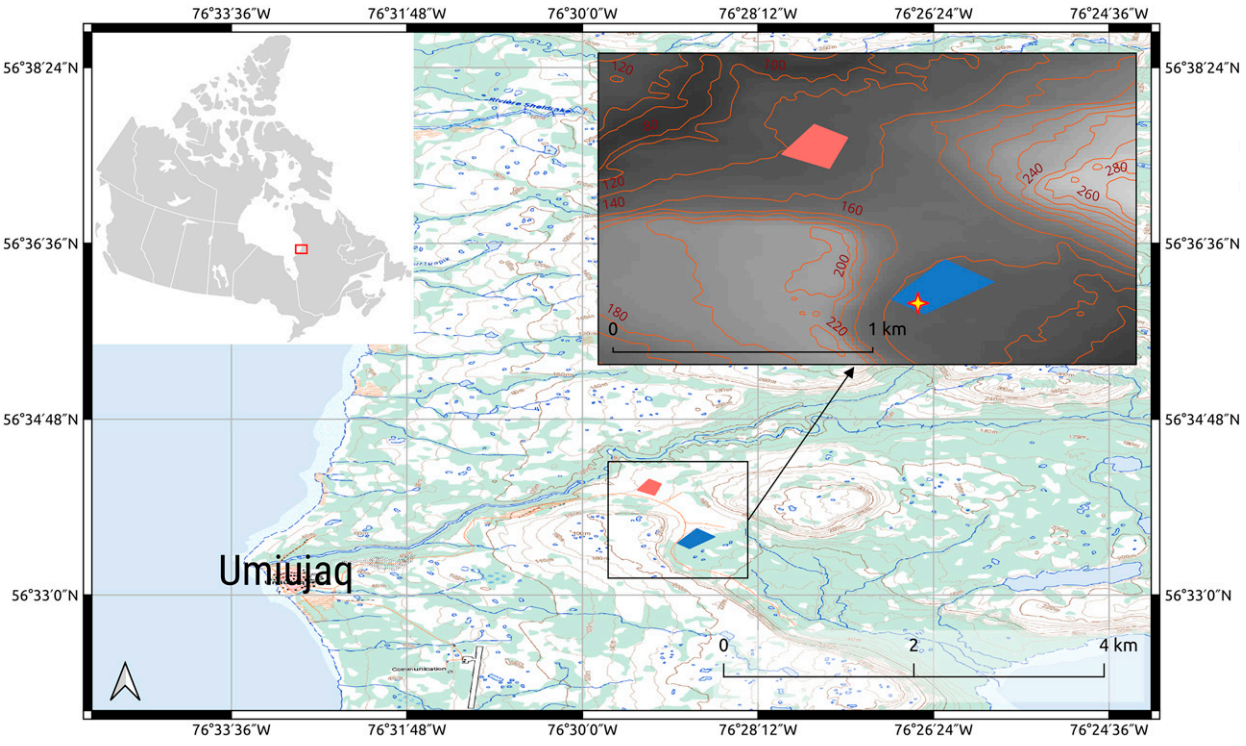

FIG. 1. Location of the two study areas near Umiujaq, northern Quebec, Canada. The star in the South site indicates the meteorological station. Contour lines: 20 m. Map sources: atlas: Natural Resources Canada (http://atlas.gc.ca/toporama/en/index.html), overview: Lokal_Profil (CC-BY-SA-2.5), DTM and contour lines: Natural Resources Canada.

The North site is centered around 56.5684°N, 76.4895°W (elevation 122 m) and the South site around 56.5594°N, 76.4816°W (elevation 133 m). The centers of both sites are 1080 m apart. The South site features lichen tundra (*Cladonia* spp., mostly *C. stellaris* and *C. rangiferina*), always accompanied with herbaceous species, mostly *Carex* sp., low and medium shrub tundra (*Betula glandulosa*, 0.2–1 m high, with some shorter *Vaccinium* sp., 0.1–0.25 cm high) and a few small thickets of krummholz spruce (*Picea mariana*, up to 2.5 m high), as detailed in Gagnon et al. (2019). This site is equipped with extensive meteorological, snow and soil monitoring instruments (Domine et al. 2015), including shortwave and longwave radiation, snow height, snow and soil temperature, and thermal conductivity. Complete meteorological data since 2012 except wind direction are reported in Lackner et al. (2022). Wind direction at 10-m height is available at https://nordicana.cen.ulaval.ca/dpage.aspx?doi=45120SL-067305A53E914AF0. The North site has in general taller vegetation and also features willow shrubs (*Salix* spp., mostly *S. planifolia* and *S. glauca*) and more extensive areas of krummholz spruce. The North site is on the west side of the pass between Hudson Bay to the west and Lake Tasiujaq (formerly Lake Guillaume-Delisle) on the east, while the South site is on the east side of the pass. Photographs of the sites are shown in Fig. 2 and Fig. S1 in the online supplemental material. There are no meteorological instruments on the North site, but frequent visits there and discussions with the locals indicate that the North site is significantly windier than the South site.

The snow supply here is probably much less limited than at other sites where snow–shrub interactions have been studied (Essery and Pomeroy 2004; Liston et al. 2002; Sturm et al. 2001). This is because of the presence of Hudson Bay to the west and of Tasiujaq Lake to the east, and also to the widespread presence of barren or lichen tundra expanses on the cuestas surrounding our site and on many parts of the valley.

b. *Experimental methods*

1) OVERVIEW

The principle of snow height mapping using a UAV is to obtain a digital terrain model (DTM) in winter and another one in summer. Subtracting the summer from the winter DTM yields snow height. The lidar beam is reflected by both the vegetation and the ground, allowing the determination of the DTM as well as the digital surface model (DSM), which represents the top of the vegetation. Subtracting the DTM from the DSM yields a map of the vegetation height in summer and of vegetation protruding above the snow in winter (Deems et al. 2013; Harder et al. 2020).

2) LIDAR SURVEYS

Both lidar surveys used a YellowScan Surveyor (16 lasers) lidar system (https://www.yellowscan-lidar.com/, last accessed on 30 August 2022) operating at 903 nm, ensuring good reflection by both snow and vegetation. Furthermore, at this IR wavelength, radiation penetration in snow is <1 cm (Deems et al. 2013), so that the actual snow surface can be determined

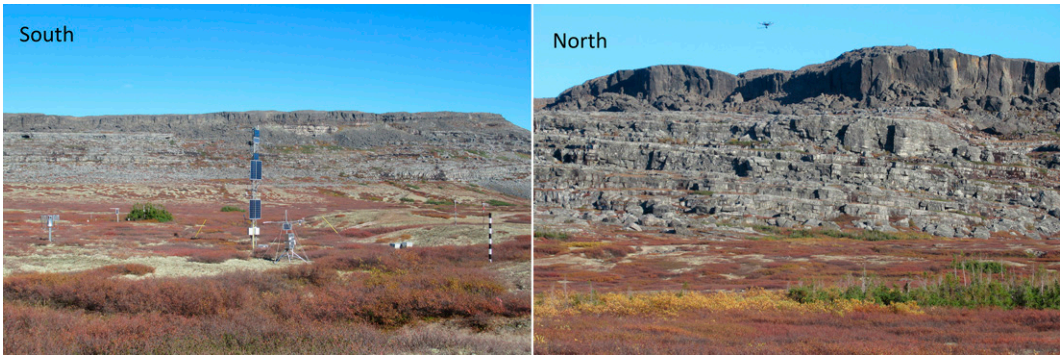

FIG. 2. (left) South site showing the various vegetation covers: lichen, low- to medium-size birch shrubs, and two spruce thickets. Lithalsas are visible on the right of this photograph. (right) North site showing birch shrubs, willows with yellow leaves, and more abundant spruce. Lichens are also present. Photographs taken on 28 Sep 2017 during the lidar survey.

with an excellent accuracy. The lidar was mounted on a DJI Matrice 600 Pro (user manual: https://manuals.plus/dji/matrice-600-pro-manual.pdf, last accessed on 30 August 2022). The lidar system is an all-integrated solution that includes laser scanner, Global Navigation Satellite System–Inertial Navigation System (GNSS-INS), embedded computer and batteries and is capable of 600 000 shots per second. The laser scanner data are coupled with the Applanix APX-15 GNSS-INS that records the position and inertial data of the lidar system. The drone was also equipped with a DJI Zenmuse X3 camera for FPV (first-person view) purposes to ensure the safety of the equipment and the crew.

All flights were done in automatic mode. UAV takeoffs and landings were done in manual mode as well as the initialization of the GNSS-INS platform integrated in the lidar system before and after data acquisition. During data acquisition, the UAV flight speed was set to 5 m s^{-1} and the altitude was set to 40 ± 5 m above ground. For the lidar data, a minimum lateral overlap of 50% between scans is respected. Flights had a maximum duration of 15 min and covered areas of 4 ha (North site) and 6 ha (South site). The snow-free survey was performed on 28/29 September 2017 and the snow survey on 25/26 April 2018.

3) GEOREFERENCING

To georeference the lidar point cloud, a GNSS base station was installed on a geodesic benchmark (point 83KP057 from Natural Resources Canada) at approximately 2-km distance from the area of interest (AOI). Raw GNSS data collected by the base station throughout the entire duration of the flights and for a minimum of at least 5 h is then postprocessed with Rinex data from the Canadian Spatial Reference System Precise Point Positioning (CSRS-PPP) of Natural Resources Canada (NRCan) to get the precise position of the base, with an uncertainty on the position better than 1.15 cm. The coordinates in the vertical Canadian datum GCVD28 (used hereinafter for all coordinates) were then calculated with the PPP tool from the NRCan CRSP-PPP online service and the latitude and longitude of the 83KP057 geodesic benchmark was validated in terms of accuracy. The final accuracies of the geodetic benchmark were 0.009 m in latitude and 0.011 m in longitude.

The first quality control to validate lidar acquisitions was through the precision of the postprocessed trajectories of the UAV. The root-mean-square (RMS) error for each component (north, east, and down) needed to respect the expected values of a Global Navigation Satellite System–Post Processed Kinematic (GNSS-PPK) positioning, which are 2 cm for north and east components and 3 cm for the vertical component. These RMS errors were satisfied in all UAV flights processed in this work.

For both surveys (snow-free and the snow-covered UAV flights), to control the accuracy of the final point clouds, five check ground control point (GCP), using high reflective targets (with size 1.21 m × 0.61 m), were installed before the flights in representative sectors of the terrain. The four corners of each target were measured with a GNSS-RTK (Real-Time Kinematics) rover connected to the GNSS base station.

The next quality control was the validation of the point cloud georeferencing which was performed by comparing the position of the check GCP corners and their positions in the point clouds. The latter was displayed on intensity mode to see the high reflective targets. The three components of each corner (XYZ) of the point clouds were compared to their appropriate values measured with the GNSS-RTK rover. The mean geolocation errors on the components of the five GCPs were below 2.8 cm in X, 3.1 cm in Y, and 4.4 cm in Z for the two lidar acquisitions (summer and winter).

The digital terrain model was also checked by comparing the value XYZ of the check GCPs to their appropriate value on the surface, which had an RMS below 5 cm.

The GCP validation of summer and winter point clouds derived from the UAV lidar system are equivalent to the accuracies obtained in previous works based in this technology (Harder et al. 2020; Koutantou et al. 2021). Despite the differences between the study areas of these works, a maximum RMS of 0.15 m in the snow and vegetation heights estimation may be expected in North and South sites.

No field validation of snow heights was performed using manual probes. Probes easily penetrate the lichen layer whose depth varies between 5 and 20 cm. Under tall shrubs the lichen is often replaced by moss, which freezes in winter and in this case, there would be no probe penetration. Probe

measurements would then have a random bias between 0 and 20 cm, greater than the expected accuracy from the lidar. This overprobing issue has already been explicitly or implicitly encountered in previous studies. Proulx et al. (2022) observed that lidar snow heights were lower than manual measurements and attributed this to overprobing into leaf litter. Harder et al. (2020) compared lidar and manual snow height measurements and almost always obtained greater heights with manual measurements. Although they do not specifically identify overprobing into soft layers as the cause, it appears as the most likely reason. Considering the highly variable nature of the surface litter/vegetation layer at our site, the interest of manual validation measurements is therefore very limited. Moreover, the uncertainty associated not only to probe measurements but also to the probing spot positioning (usually based on manual GPS devices) also introduces more noise to this evaluation and require a comparison over extended areas to evaluate the spatial variability of both manual and lidar snow height acquisitions (Revuelto et al. 2014).

We can, however, compare the lidar value with that of our SR50 acoustic snow gauge. The gauge value is 1.14 m. For the 30-cm diameter circle just below the gauge, lidar values are in the range 1.02–1.15 m, with an average of 1.07 m. This shows that even though it is a single point observation, both snow height observations are in good agreement, especially considering that the penetration depth of the lidar and ultrasonic beams in lichen may be different. Additionally, lidar observations also have intrinsic errors. For instance, the laser beam divergence has an associated elliptical footprint within which multiple returns can be retrieved from different objects (soil surface, bush branches, leaves, etc.), which then might be interpreted as a single point that has multiple returns (Deems et al. 2013). Similarly, the georeferencing of the point cloud or the minor penetration that the laser beam might have on different surfaces impact the overall accuracy of airborne lidar observations. Nonetheless, if a well-established acquisition and processing protocol is followed, lidar snow height deviations from manual measurements are expected to be low (<10 cm in no lichen/moss areas) as previous works have shown in other study areas with contrasted differences (Currier and Lundquist 2018; Harder et al. 2020; Jacobs et al. 2021; Mazzotti et al. 2019).

Last, to support this accuracy estimate, we estimated lidar returns in representative areas of the South site by selecting an area with mostly birch and another area with mostly lichen. In the birch-dominated area, the average point cloud density was 540 points m^{-2} for points classified as lichen, 750 points m^{-2} for low vegetation points (grasses and very small shrubs such as *Vaccinium* sp.) and 2540 points m^{-2} for those classified as birch (*Betula glandulosa*). In the lichen-dominated area, the average point cloud densities were 1500 points m^{-2} for lichen classified points and 770 points m^{-2} for grasses and low shrub points. These high point cloud densities guarantee the reliable computation of snow and vegetation heights at 10-cm spatial resolution, with an estimated accuracy around 10 cm, equivalent to similar studies.

4) AUTOMATIC CLASSIFICATION OF TERRAIN TYPES

The points clouds obtained in the different UAV flights were classified using an automatic classification macro from Terra Match software. The point cloud was classified in three classes as bare ground, vegetation, and others. If the automatic classification method did not perform properly, manual classification was done to ensure the right delimitation of each class.

5) SNOW COVER THICKNESS CALCULATION

The first step was to create two digital terrain models (DTM) using the bilinear interpolation method to finally produce 10-cm spatial resolution maps DTM. To interpolate a pixel located between a 10-cm known pixels distance, we calculated an average between these pixels that we weight according to the distance of the interpolated pixel to each of the original pixels. In this case a bivariate function was applied. The second step was the calculation of the snow cover thickness by applying a differential between the winter DTM (snow-covered) and the fall DTM (snow-free) for generating a distribution map in which each pixel gives the value of the snow cover thickness for a given geographic location.

Both high and low branches and leaves of vegetation reflect the lidar beam. Here we define the average vegetation height over a 99 cm × 99 cm cell (referred to as 1 m for ease) as the average height of the 90th–98th percentile of vegetation height pixels (Fig. 3). Vegetation height is indeed perceived at the height of the tallest branches, but we leave out the upper percentiles to reduce the impact or very high outliers. We subsequently often consider snow height with a 1-m resolution. De Michele et al. (2016) have shown that increasing the spatial resolution of snow height maps below 1 m does not add significant information about the snow height variability.

When snow-free data were acquired on 28/29 September 2017, the foliage of the deciduous shrubs was in fall colors and part of the leaves had fallen (Fig. 2), with a leaf area index visibly under unity, ensuring that the lidar beam easily reached the ground. The limited density of spruce also allowed ground detection. During the snow season survey on 25/26 April 2018, the snowpack was almost at peak accumulation. The snow height at our automatic SR50 gauge at the southwest edge of the South site then read 1.14 m and the snow height was within 0.05 m of that value between 20 January and 13 May, when a late spring snowfall added 0.2 m of snow which quickly settled. The snow height during measurement was therefore representative of the winter. However, the 2018 snow season had a high snow accumulation when compared to other years. Peak snow was 1.0 m in 2019, 0.6 m in 2017, 0.9 m in 2016 and 2015, and 1.28 m in 2012.

3. Results

a. *Topography and distributions of snow and vegetation heights*

Figure 4 shows the summer DTM, vegetation height, and snow height maps at both sites. The North site has a very gentle slope of 1.7% to the northwest and a 4-m-deep gully on its southern edge. A readily visible part of the vegetation exceeds

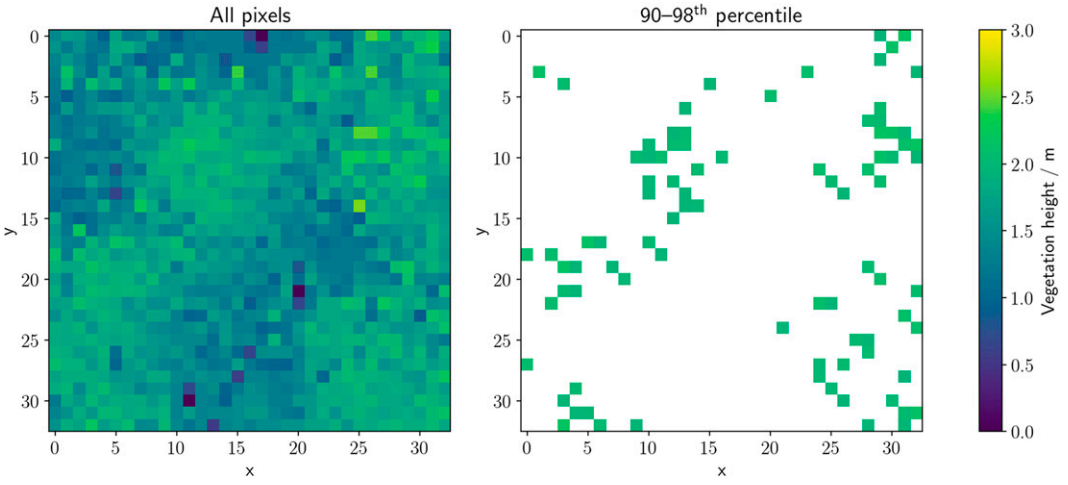

FIG. 3. Example of the resampling method of the 3-cm horizontal resolution vegetation height maps to 1 m. (left) All the pixels of the 3-cm resolution map within a 1 × 1 m^2 pixel (average vegetation height: 1.58 m). (right) The pixels retained for the averaging step (90th–98th percentile; average vegetation height: 2.04 m).

1.5 m height, because of the presence of willows and of many spruce trees. The South site has a steeper slope to the southeast in its northwest part, of 8.5%, which flattens out to 2.3% in the southeast part. There are lithalsas on its southern edge that are about 4 m high, but no well-marked gully. Vegetation exceeds 1.5 m in height only for two spruce thickets. There are no spruce beyond these thickets and no willows.

Figure 5 shows the distribution of vegetation heights at both sites and confirms the maps of Fig. 4: there is much more high vegetation on the North site, and the average height is

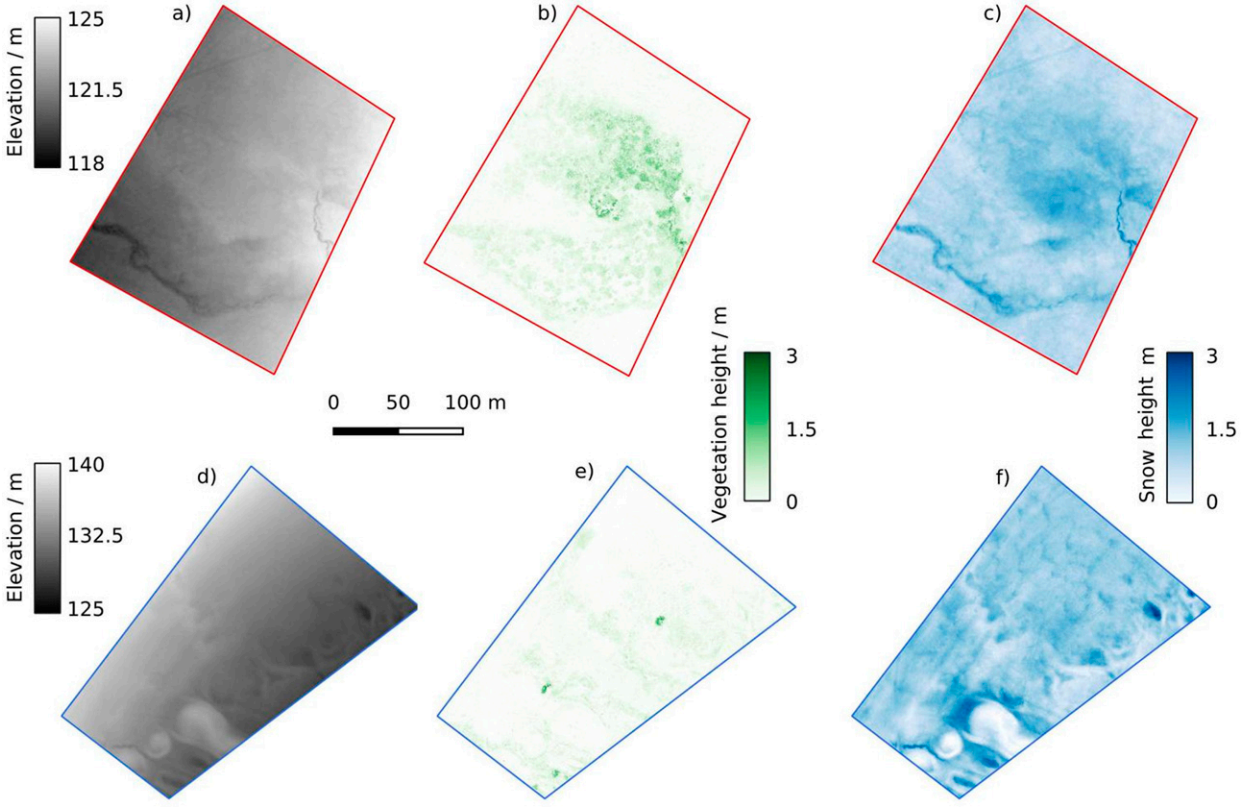

FIG. 4. (a) Elevation, (b) vegetation height using the 1-m resolution product, and (c) snow height maps of the North site. (d) Elevation, (e) vegetation height, and (f) snow height maps of the South site.

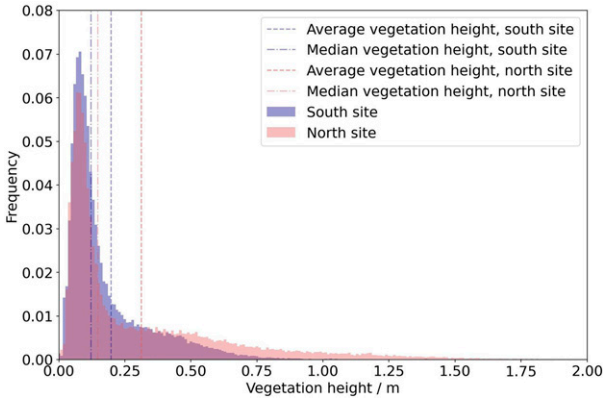

FIG. 5. Distribution of the vegetation height at both study sites, using the 1-m resolution products. The bin size of the histogram was set to 1 cm. The average, median, and mode vegetation heights are 0.19, 0.12, and 0.08 m for the South site and 0.31, 0.14, and 0.07 m for the North site. Modes are not shown for clarity.

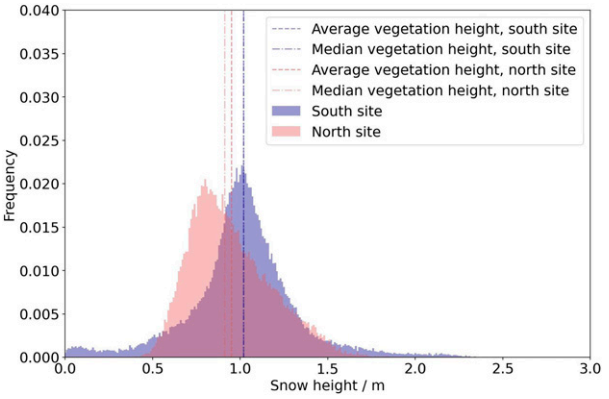

FIG. 6. Snow height distribution at both study sites, using the 1-m resolution products. The bin size of the histogram was set to 1 cm. The average, median, and mode snow heights are 1.02, 1.02, and 1.01 m for the South site and 0.95, 0.91, and 0.80 m for the North site. Modes are not shown for clarity.

0.35 m versus 0.19 m for the South site. The peak in height frequency distribution at both sites is around 0.09 m and corresponds to lichen tundra. Field observations revealed that the lichen can be up to 0.2 m thick, but it is visibly optically thick so that the lidar beam cannot penetrate 0.2 m deep. There are some grasses on lichen tundra, and given our definition of vegetation height at 1-m resolution, lichen with a few blades of grass show up as vegetation with a height around 0.09 m. There is a much wider distribution of heights at the North site, due to much more frequent tall vegetation, such as spruce and willows. At the South site, birches rarely reach 1 m in height, there are no willows, and there are only two spruce thickets where the top of trees cover at the most 200 one-meter pixels.

Despite the taller vegetation at the North site, Fig. 6 shows that snow height is lower at the North site with average, median, and mode values of 0.95, 0.91, and 0.80 m, respectively, versus 1.02, 1.02, and 1.01 m for the South site. There are striking differences in snow height distributions between both sites. There are many pixels with little or no snow in the South site, because of bumps (lithalsas) where snow is blown off. The North site distribution is more asymmetric with a tail on the greater heights side, due to the much more frequent tall vegetation.

We compared the topography of both sites using the topographic position index (TPI). The TPI "measures the relative topographic position of the central point as the difference between the elevation at this point and the mean elevation within a predetermined neighbourhood" (De Reu et al. 2013). A point at the top of a hill therefore has a positive TPI whereas a point in a hollow has a negative TPI, as clearly illustrated in Fig. 2 of Salinas-Melgoza et al. (2018). The TPI is calculated by comparing its position with points within a given distance called the search distance. TPI distributions for both sites are shown in Fig. 7, for a search distance of 31 m. The impact of other search distances is detailed in Fig. S3. The South site has higher extreme TPI values and is clearly more rugged than the North site. Figure 7 also shows that the South site has a wider TPI distribution than the North site. This is further illustrated by the box-and-whisker plot of the TPI distribution, in Fig. S2 in the supplemental material.

b. *Global correlations*

The next step is to examine correlations between snow height, vegetation height, and topography.

1) SNOW HEIGHT VERSUS VEGETATION HEIGHT

Figure 8 plots snow height as a function of vegetation height for the North site. However, using data at 1-m resolution may not be the most relevant approach. For example, snow accumulates not only within vegetation but also in the lee of protruding vegetation, as evidenced, for example, at forest edges (Currier and Lundquist 2018) and for low shrubs (Domine et al. 2016; Sturm et al. 2001). We therefore also examined pixel sizes of 10 and 20 m (i.e., spatial resolutions of 10 and 20 m). Figure 8 shows that the correlation coefficient increases significantly when larger pixels are considered. For 20-m resolution, $r = 0.80$. For the South site, however, the

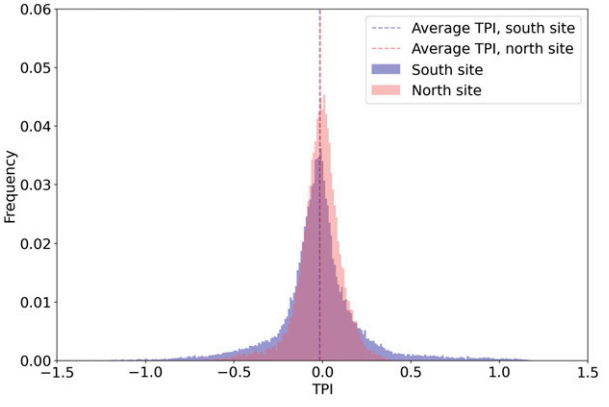

FIG. 7. TPI distribution at both study sites, using the 1-m resolution products. The TPI search radius was set to 31 m. The bin size of the histogram was set to 0.01. Both averages are nearly identical.

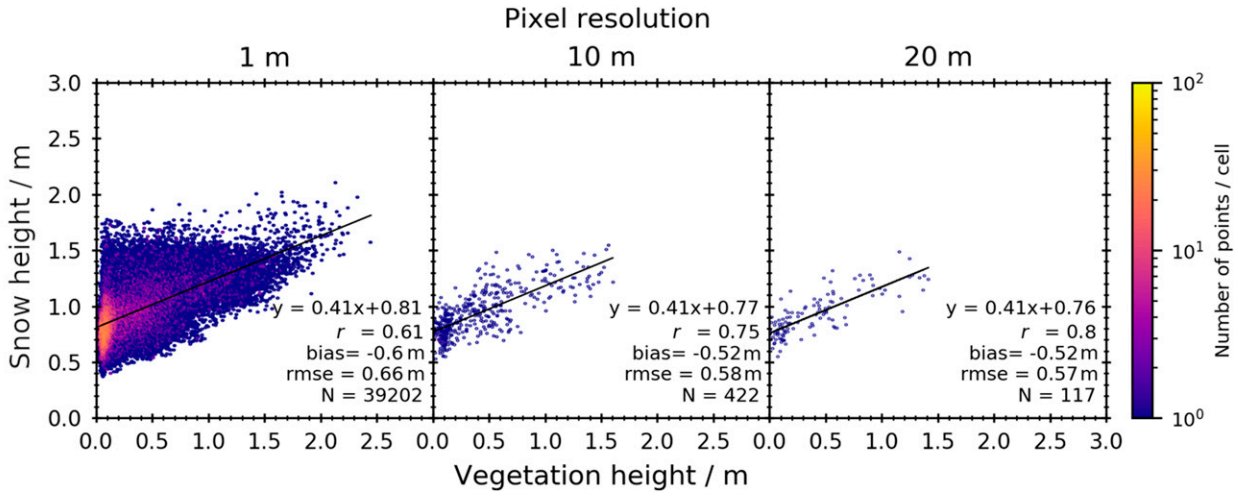

FIG. 8. Scatterplots of the relationship between vegetation height and snow height at the North site for pixel sizes of 1, 10, and 20 m. Owing to the large number of data points, the scatterplot was represented as hexbins colored by the number of data points contained within each bin. In this plot, each hexbin represents 1.5 cm × 1.5 cm. For all correlations, p values are <0.001.

correlation between snow height and vegetation height is very low (Fig. 9), as $r = 0.28$ at 20-m resolution.

2) SNOW HEIGHT VERSUS TOPOGRAPHY

Figure 10 shows a strong correlation between TPI and snow height for the South site ($r = -0.82$), but a weaker correlation for the North site ($r = -0.54$). The correlation expectedly shows greater snow heights for negative TPI values (hollows).

3) TOPOGRAPHY VERSUS VEGETATION HEIGHT

It is also relevant to investigate the correlation between topography and vegetation height as case studies have reported that vegetation could be higher in hollows (Pelletier et al. 2019). Figure 11, however, shows a fairly symmetrical distribution of vegetation heights around TPI = 0. There is only a very slight tendency for vegetation to be higher for negative TPI values, but r values are very low ($r = -0.08$, North site and $r = -0.13$, South site) for the TPI with a 31-m search distance. Any value of the search distance leads to a similar conclusion. Figures S4 and S5 show correlation using the TPI with 5- and 10-m search distances, with r values lower than 0.1. There is no well-marked trend for taller vegetation in hollows.

4) MULTIVARIATE CORRELATIONS

To test for the combined effects of vegetation height and topography on snow height, snow height is plotted as a function of TPI for different ranges of vegetation height or the North and South sites (Fig. 12). In the North site, taller vegetation and more negative TPI values combine to produce thicker snow. However, in the South site, there is no obvious impact of vegetation height on snow height, in addition to the impact of the TPI.

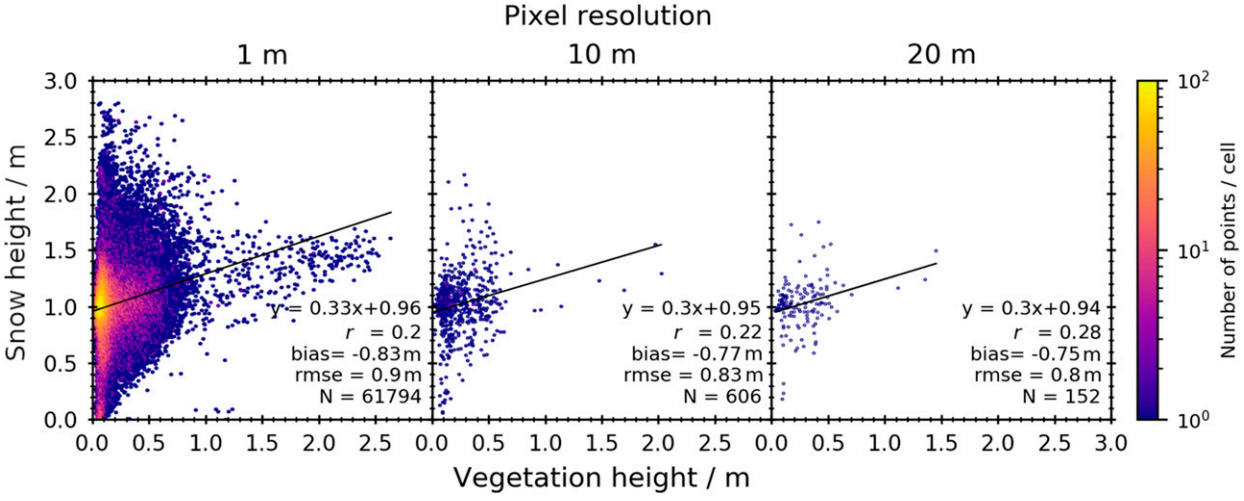

FIG. 9. Scatterplots of the relationship between vegetation height and snow height at the South site for pixel sizes of 1, 10, and 20 m. For all correlations, p values are <0.001.

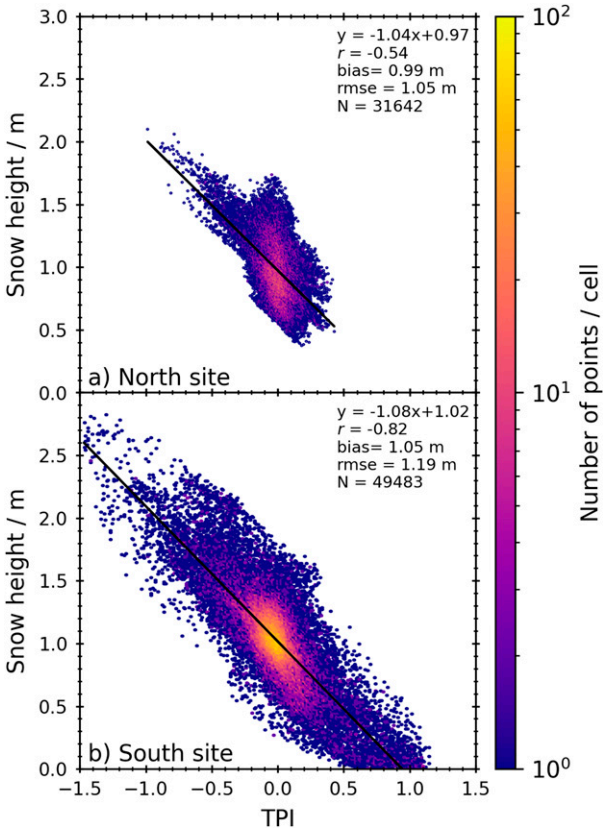

FIG. 10. Scatterplots of the relationship between TPI with a search distance of 31 m and snow height at (a) the North site and (b) the South site. The p values are all <0.001.

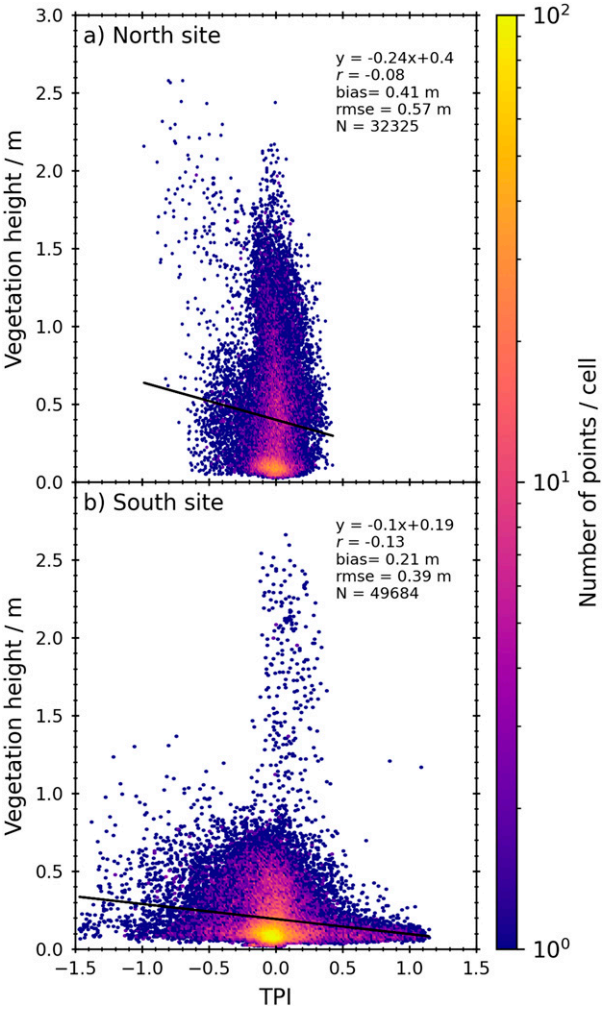

FIG. 11. Scatterplots of the relationship between TPI with a search distance of 31 m and vegetation height at (a) the North site and (b) the South site. The p values are all <0.001.

These multivariate correlations are even more clearly evidenced in the 3D plots shown in Fig. 13, for 1-m pixels and with the TPI calculated with a 31-m search distance. Views along the axis of the correlation plane are shown in Fig. S6 to reveal residuals. For the North site, Fig. 13a, the addition of vegetation height to the TPI to predict snow height increases the determination coefficient R^2 from 0.29 to 0.59, a large improvement. This is not surprising since vegetation height is also a good predictor of snow height, with $R^2 = 0.37$ (Fig. 8). For the South site, however, R^2 increases only from 0.672 to 0.675 when two predicting variables are used, a negligible improvement. This is expected since vegetation height is here a poor predictor of snow height, with $R^2 = 0.04$ (Fig. 9). TPI is clearly the main predictor of snow height in the South site, while vegetation height is the main predictor in the North site. Table 1 sums up correlations for both sites.

5) SUMMARY OF MAIN CORRELATION CONCLUSIONS

To sum up observations, it is interesting to stress the differences between both sites. The North site is windier, has taller vegetation, is less rugged, and has less snow than the South site. In the North site, snow height is strongly correlated with vegetation height but less correlated with topography as smoother terrain is observed here. However, the multivariate analysis shows that combining TPI and vegetation height better predicts snow height than vegetation height alone. The South site shows different effects. There, snow height is strongly correlated with topography, probably accounting for the higher terrain heterogeneity that characterizes this site, and shows almost no correlation with vegetation height. Combining vegetation height with TPI to predict snow height only leads to a negligible improvement over TPI alone.

c. *Process studies*

General correlations are useful for an overview of interactions, but a more detailed understanding benefits from the examination of selected cases. Below, we present transects with profiles of relevant variables: summer and winter DTM, summer DSM, snow and vegetation heights, and TPI computed for the best search distance (31 m). The representativity of a single transect line may be questioned, as, for example, a tall shrub just next to that line could affect snow height

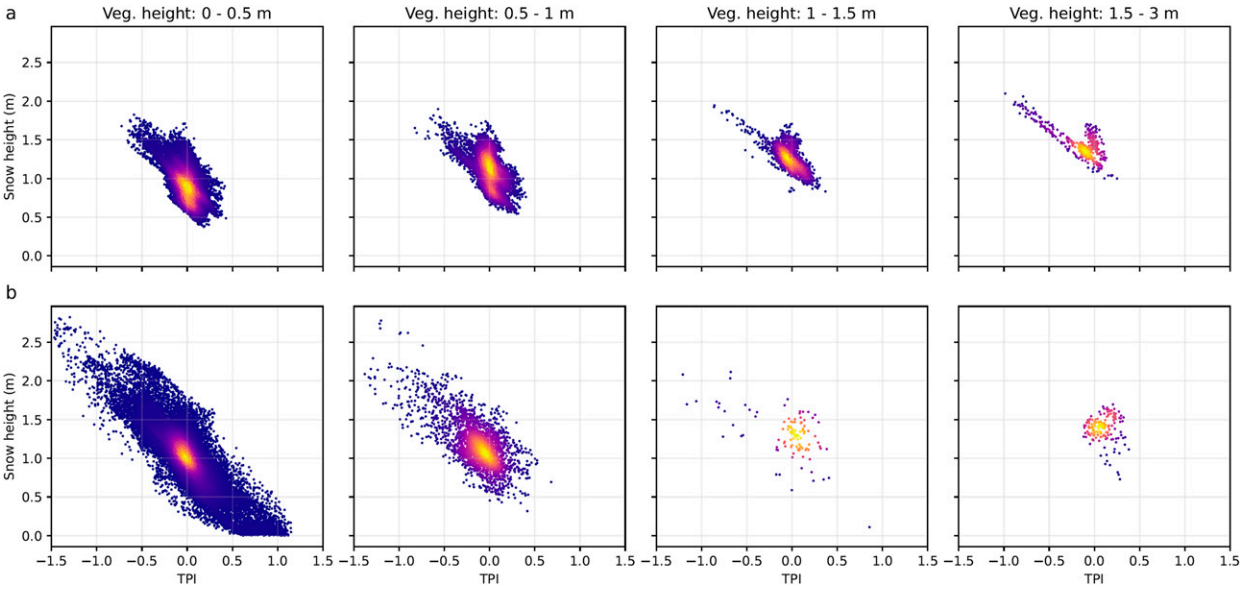

FIG. 12. Scatterplots of the relationship between TPI and vegetation height for (a) the North site and (b) South site. This is similar to Fig. 10, but with vegetation heights binned in 0.5–1.5-m ranges. The color scale is similar to Fig. 10.

without showing up on our profiles. In each case we therefore investigated eight parallel profiles 0.5 m apart. Each profile is shown in a light color and the average in a dark color. For each average profile of snow height, vegetation height, and TPI, we calculated the determination coefficient between these three variables, which are summed up in Table 2. We stress that the transects selected here are to illustrate specific processes are not meant to be representative of both areas studied.

1) NORTH SITE TRANSECTS

Figure 14 shows transects over an extended patch of medium to tall vegetation comprised of spruce, willows, and some birch. The deepest snow coincides with the tallest vegetation and with a well-marked hollow (the lowest TPI in this transect). Snow height is reasonably well correlated to vegetation height ($R^2 = 0.25$) and to TPI ($R^2 = 0.37$). Combining both vegetation height and TPI to predict snow height improves the correlation ($R^2 = 0.64$). Correlation coefficients, as well as the trivariate best-fit correlation linking snow height to vegetation height and TPI, are summed up in Table 2.

Transect 2 (Fig. 15) is over mixed vegetation comprised of birch as well as spruce and willows and with more varied topography. The distance range 140–180 m shows that vegetation causes accumulation potentially up to 20 m from the spruce patch. When vegetation is lower, as at the start of the transect, the effect of topography is obvious with snow accumulation in a hollow. On this transect with large variations in vegetation height and little topography, the correlation is

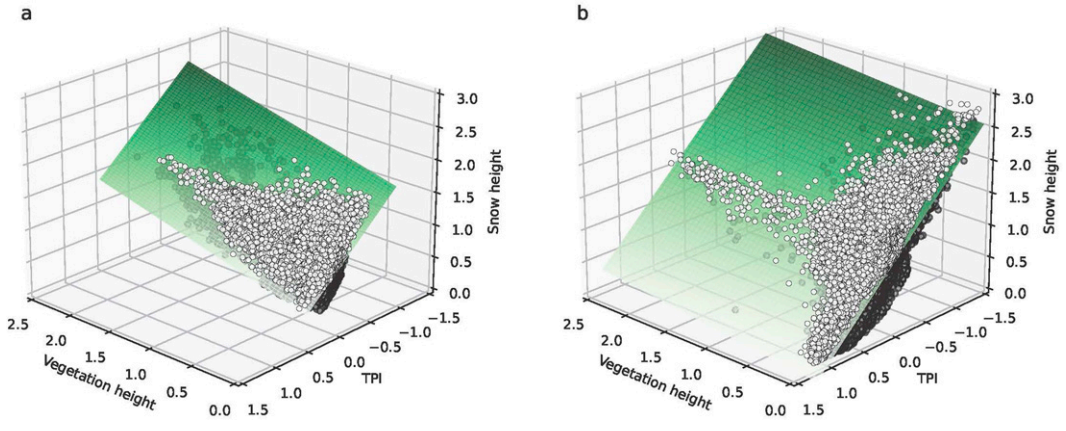

FIG. 13. 3D plot of the combined impact of TPI and vegetation height on snow height. Open circles are above the plane; closed circles are below the plane. (a) North site. The equation of the best-fit correlation plane is snow height = 0.3592 × vegetation height − 0.9500 × TPI + 0.8288, with $R^2 = 0.594$. (b) South site. The equation of the best-fit correlation plane is snow height = 0.1485 × vegetation height − 1.0640 × TPI + 0.9876, with $R^2 = 0.675$.

TABLE 1. Correlation parameters between vegetation height, snow height, and TPI (search radius of 31 m) for the North and South sites. Bivariate and trivariate R^2 values are shown. The coefficients for the best-fit equation, snow height = $A \times$ vegetation height + $B \times$ TPI + C, are also shown.

	Bivariate R^2				Trivariate coefficients		
Site	Vegetation–snow	TPI–snow	Vegetation–TPI	Trivariate R^2	A (vegetation height)	B (TPI)	C (constant)
North	0.372	0.292	0.006	0.594	0.3592	−0.9500	0.8288
South	0.040	0.672	0.017	0.675	0.1485	−1.0640	0.9876

much more marked with vegetation (R^2 = 0.44) than with TPI (R^2 = 0.05). While some intuitive correlation with topography appears upon visual inspection, statistics indicate that this correlation is in fact masked by the much greater effect of vegetation. The trivariate correlation is significantly improved over bivariate ones, with R^2 = 0.65 (Table 2).

The originality of transect 3 (Fig. 16) is that there is no protruding vegetation. Data between 0 and 35 m show that the snow surface is smooth over variable vegetation, suggesting that once vegetation is covered, its impact on snow height is reduced. The topography is rather smooth, and the one significant hollow features the greatest snow height. In those peculiar conditions, the correlation with vegetation height is low (R^2 = 0.143) while that with TPI is very high (R^2 = 0.96). Contrary to the previous transect, vegetation effects do not mask the impact of topography, leading to a high correlation between topography and snow height. The trivariate correlation is therefore not improved over that with TPI alone (Table 2).

Transect 4 (Fig. 17) is across a gully. Both sides of the gully have little erect vegetation, with mostly lichen, while the gully itself harbors low shrubs. The snow surface is smooth and does not reveal the presence of underlying elements. The snow height is greatest over the gully and expectedly is highly correlated with TPI (R^2 = 0.95) and also well correlated with vegetation height (R^2 = 0.64), since vegetation and TPI are well correlated (R^2 = 0.66). The trivariate correlation is not improved over the TPI one (Table 2) because snow height and TPI are already well correlated.

To sum up our observations of the North site, when there are varied vegetation heights with protruding vegetation, snow height correlates well with vegetation height. When vegetation does not protrude, its impact on snow height is reduced. Topography does affect snow height, but this correlation can be masked by the greatest impact of vegetation height at this North site. Topography and vegetation interact, as illustrated in transect 4, where a hollow and higher vegetation coincide, and both vegetation and TPI are correlated with snow height. Trivariate correlations are improved over bivariate ones only when TPI and vegetation heights are little correlated (Table 2).

2) SOUTH SITE TRANSECTS

The South site features much less tall vegetation than the North site (Fig. 5) except for two spruce thickets (Fig. 2). However, it features a more heterogeneous topography. We first explore the main part of the area before studying the effect of the thickets.

Transect 5 (Fig. 18) investigates a line with low, nonprotruding vegetation and marked topography with a 1-m-high bump next to a slight hollow. Data confirm the observation at the North site, i.e., that nonprotruding vegetation has little impact on snow height (R^2 = 0.002). Without any significant effect of vegetation, the correlation between TPI and snow height is obvious (R^2 = 0.64). The trivariate correlation is expectedly not improved over the TPI one (Table 2).

Transect 6 (Fig. 19) was chosen to confirm the conclusions of transect 5. We again chose a line with low, nonprotruding vegetation. However, in this case, we selected a place with no well-marked topography. We again have a fairly smooth snow surface with mild wind structures that are unaffected by vegetation (R^2 = 0.002) while what little topography exists does affect snow height, as snow accumulates in the small hollows (R^2 = 0.48). TPI and vegetation height are not correlated,

TABLE 2. Correlation parameters between vegetation height, snow height, and TPI (search radius of 31 m) for the 8 transects presented in Figs. 14–21. Bivariate and trivariate R^2 values are shown. The coefficients for the best-fit equation, snow height = $A \times$ vegetation height + $B \times$ TPI + C, are also shown.

		Bivariate R^2				Trivariate coefficients		
Transect No.	Site	Vegetation–snow	TPI–snow	Vegetation–TPI	Trivariate R^2	A (vegetation height)	B (TPI)	C (constant)
1 (Fig. 14)	North	0.253	0.373	0.000	0.639	0.5981	−1.3097	0.8858
2 (Fig. 15)	North	0.440	0.053	0.099	0.654	0.5869	−0.8631	0.8048
3 (Fig. 16)	North	0.139	0.964	0.128	0.965	−0.0128	−0.7967	1.2691
4 (Fig. 17)	North	0.635	0.950	0.661	0.950	0.0353	−0.9362	0.8462
5 (Fig. 18)	South	0.002	0.642	0.004	0.642	−0.0130	−1.0234	1.0087
6 (Fig. 19)	South	0.002	0.482	0.001	0.483	0.0261	−1.1689	1.0671
7 (Fig. 20)	South	0.096	0.135	0.063	0.186	0.3863	−0.2158	0.9432
8 (Fig. 21)	South	0.220	0.009	0.081	0.277	0.5182	−0.7123	1.0187

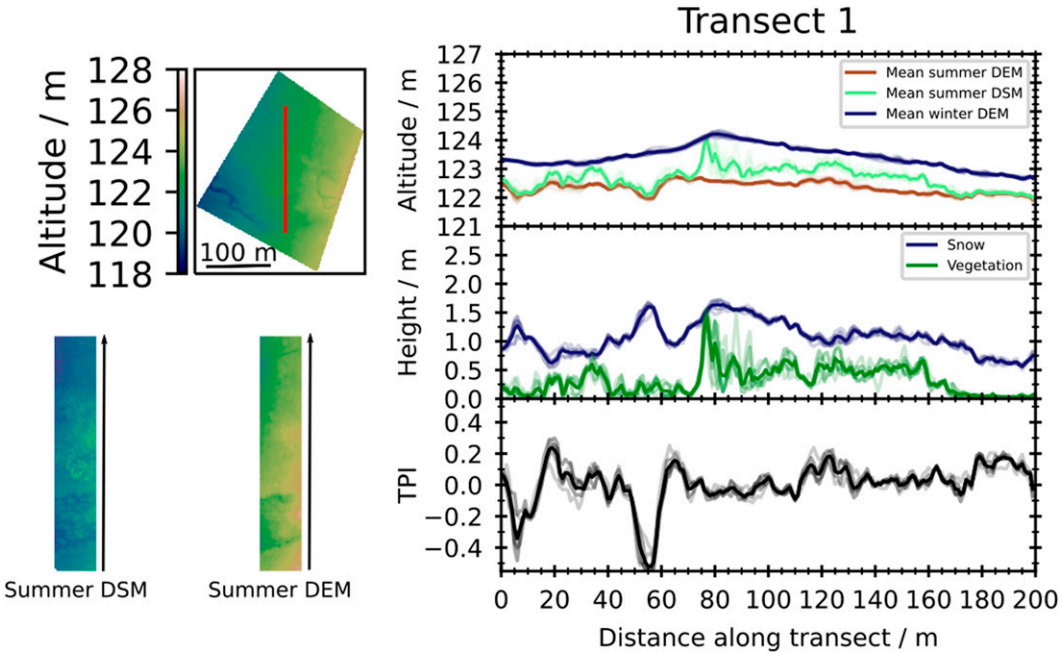

FIG. 14. Transect 1 in North site. Eight transects of 200 m in length evenly distributed over a width of 4 m, as well as their average values are shown. The start point of the averaged eight parallel transects is 56.56755°, −76.48844° [World Geodetic System 1984 (WGS84)]. The direction drawn is from south to north (0°). The top-left color scale applies to the three color graphics at the left of the figure. DEM stands for digital elevation model, which is equivalent to DTM.

and again the trivariate correlation is not improved over the TPI one (Table 2).

Transect 7 (Fig. 20) is fairly similar to transect 6, with no protruding vegetation, but it is on a slope. Again, the best predictor of snow height is the TPI ($R^2 = 0.14$) but since there is a slight correlation between TPI and vegetation ($R^2 = 0.06$), the determination coefficient between snow height and vegetation height is 0.10. The trivariate correlation is therefore slightly

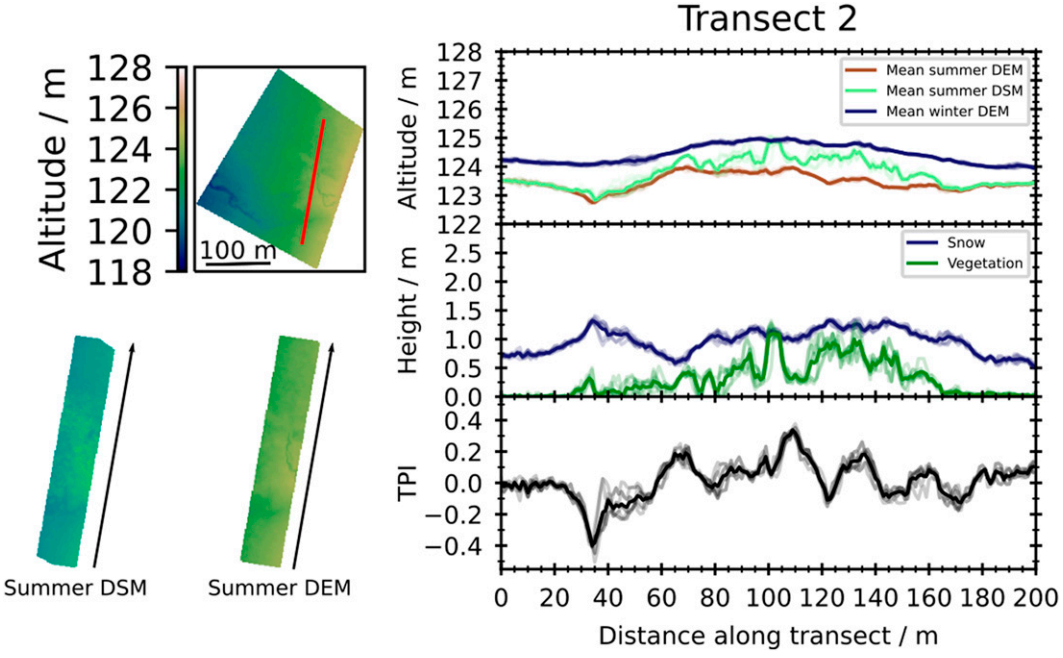

FIG. 15. Transect 2 in North site, as in Fig. 13. The start point of the averaged 8 parallel transects is 56.56735°, −76.4800° (WGS84). The direction drawn is from south to north (10°).

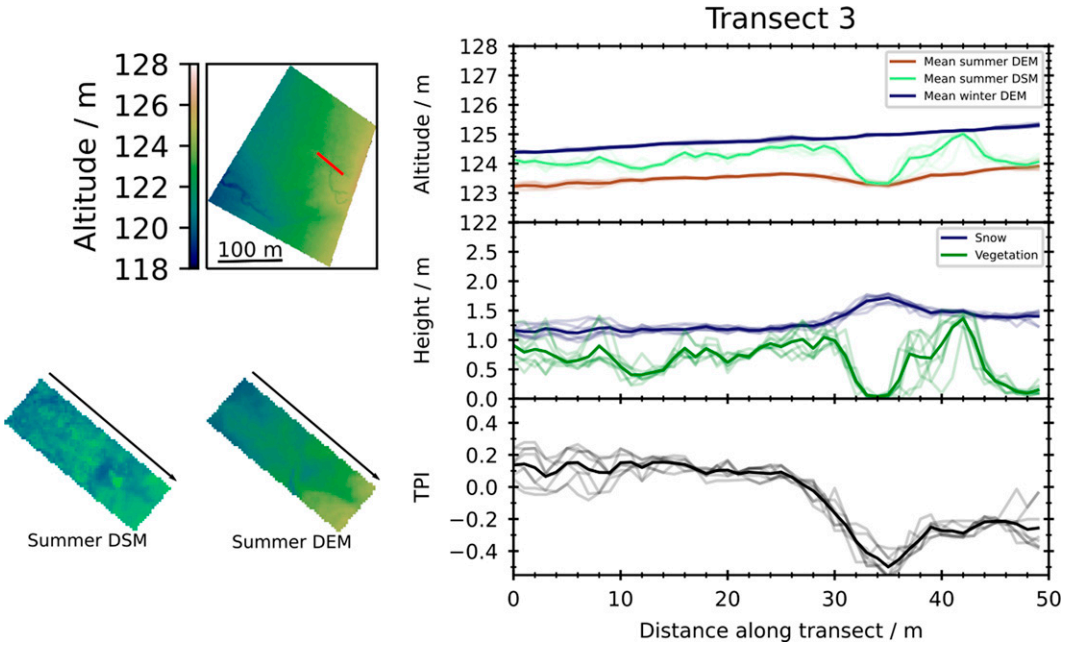

FIG. 16. Transect 3 in North site, as in Fig. 13, but over a 50-m distance. The start point of the averaged eight parallel transects is 56.56845°, −76.48758° (WGS84). The direction drawn is from northwest to southeast (130°).

improved over the TPI one alone (R^2 = 0.19). The correlation between snow height and topography is much lower than for transects 5 and 6. We hypothesize that this is due to random variation in the positions of wind structures such as sastrugi. The wind rose in Fig. S7 indeed shows that the main wind direction in the two months prior to the snow season survey was parallel to the transect, which would maximize the visibility of wind effects on the snow surface. These wind-induced surface structures

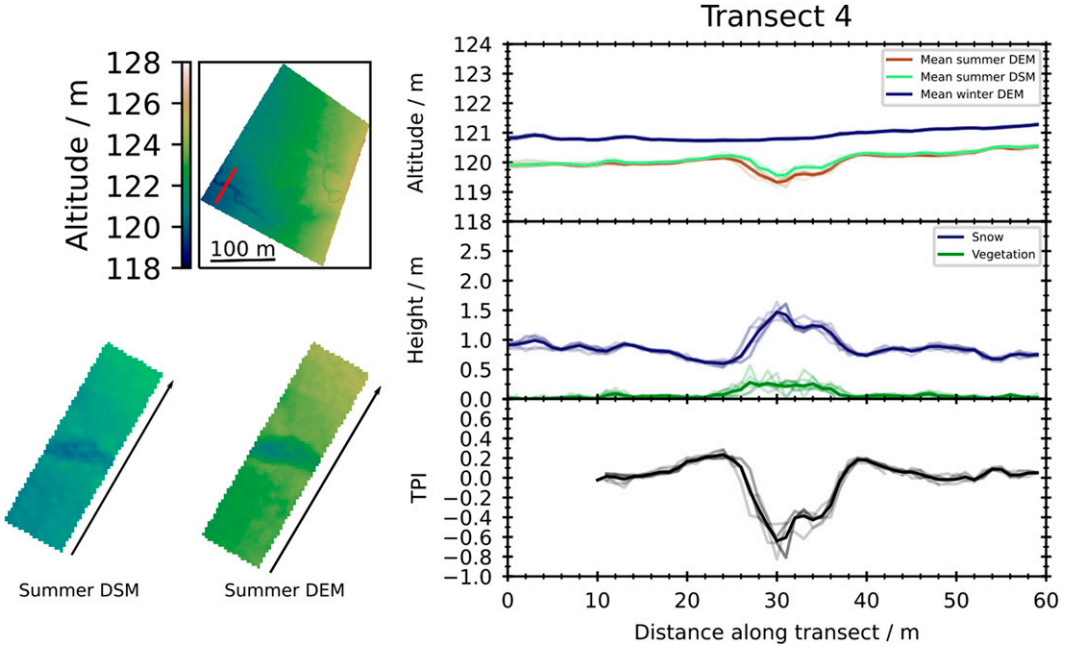

FIG. 17. Transect 4 in North site, as in Fig. 13, but over a 60-m distance. The start point of the averaged eight parallel transects is 56.56812°, −76.49012° (WGS84). The direction drawn is from southwest to northeast (30°). Owing to the proximity to the edge of the raster and a search radius of 31 m, the TPI could not be computed for the first 10 m of the transect.

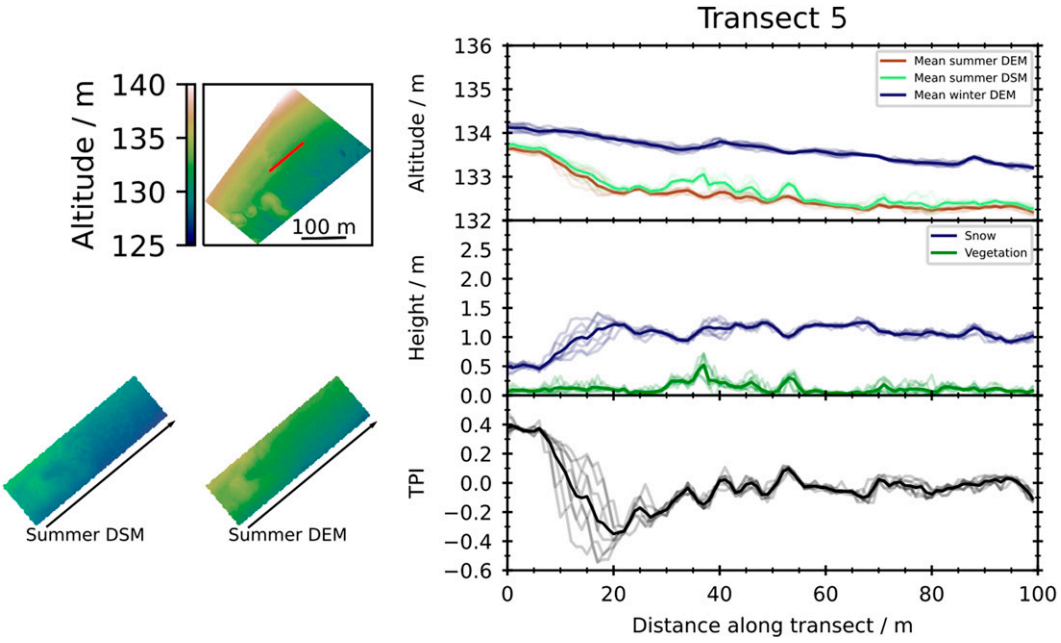

FIG. 18. Transect 5 in South site. Eight transects of 100 m in length evenly distributed over a width of 4 m, as well as their average values are shown. The start point of the averaged eight parallel transects is 56.55952°, −76.48122° (WGS84). The direction drawn is from west-southwest to east-northeast (50°).

then partly mask the effect of topography and explain the low correlation.

These transects all indicate that when vegetation height is much lower than snow height, there is very little impact of vegetation on snow height. The impact of topography is then readily visible, and the effect of well-marked topography (transect 5) strongly manifests itself. When topographic variations are more limited, the correlation between TPI and snow height decreases and can be masked by wind-induced surface structures such as sastrugi. We now examine the impact of the spruce thickets.

Transect 8 (Fig. 21) is across one of the two spruce thickets of the site, essentially parallel to the contour lines. Clearly,

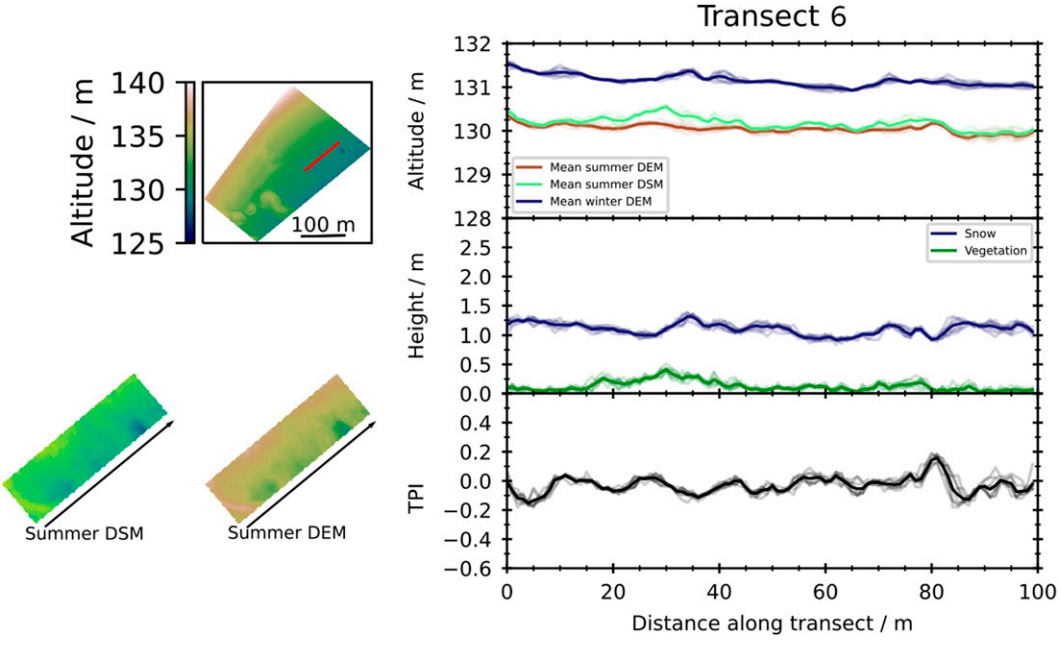

FIG. 19. Transect 6 in South site, as in Fig. 17. The start point of the averaged eight parallel transects is 56.55948°, −76.47983° (WGS84). The direction drawn is from west-southwest to east-northeast (50°).

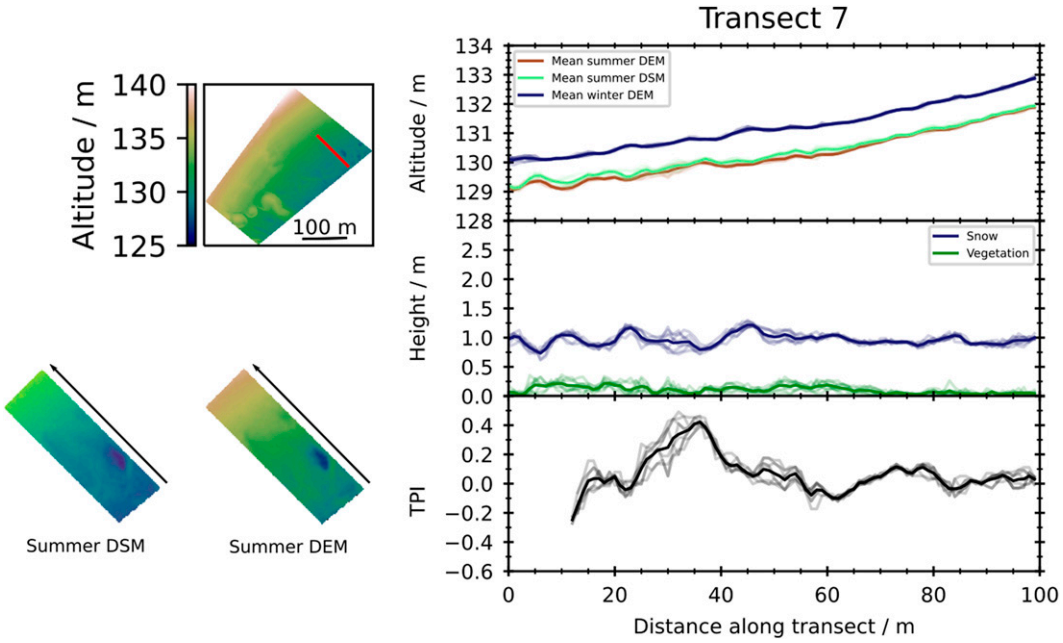

FIG. 20. Transect 7 in South site, as in Fig. 17. The start point of the averaged eight parallel transects is 56.55962°, −76.47827° (WGS84). The direction drawn is from southeast to northwest (315°). Owing to the proximity to the edge of the raster and a search radius of 31 m, the TPI could not be computed for the first 10 m of the transect.

the effect of the thicket extends far away from it. To the southwest, extra snow accumulation is visible about 50 m from the thicket edge. Time lapse photographs reveal that snow accumulation around the thicket took place early in the snow season, mostly before mid-December 2017. By the end of January 2018, the snow height was close to that during the April 2018 survey. The wind roses of Figs. S8 and S9 show that the main wind directions during both these periods were from the southwest and southeast, explaining this accumulation. While the impact of the thicket on snow accumulation is very obvious in Fig. 21, the high snow accumulation on low vegetation next to the spruce reduces the correlation between

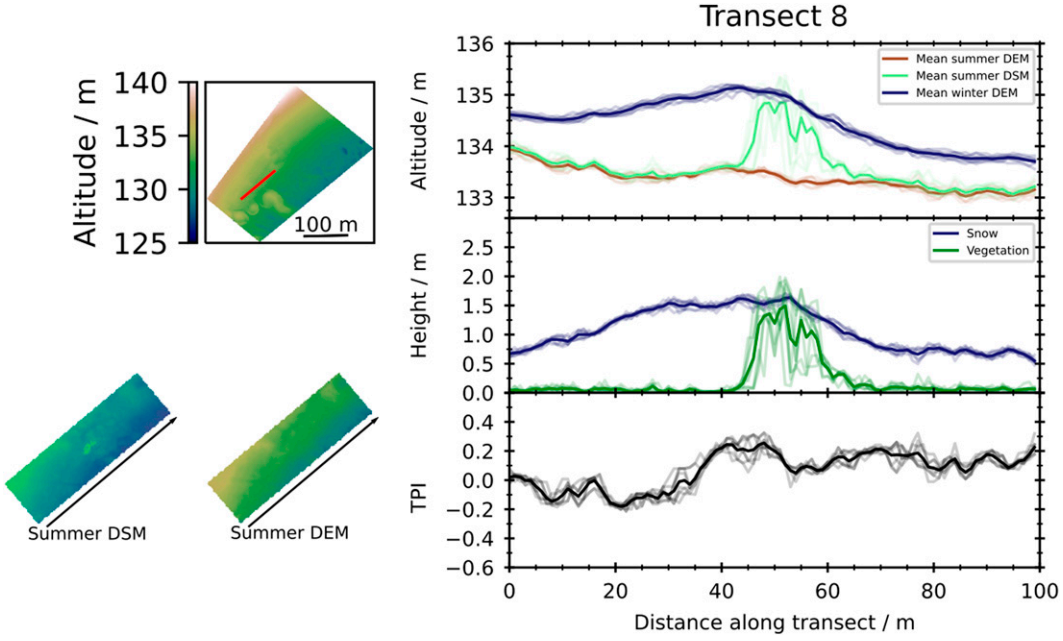

FIG. 21. Transect 8 in South site, as in Fig. 17. The start point of the averaged eight parallel transects is 56.55887°, −76.4854° (WGS84). The direction drawn is from west-southwest to east-northeast (50°).

vegetation and snow heights to $R^2 = 0.22$. The strong impact of the thicket totally masks the effect of the moderate topographic features on snow height ($R^2 = 0.01$ with TPI).

To sum up our observations of the south site, data confirm that when vegetation does not protrude above the snow, its impact on snow height is very small and snow height is then well correlated with topography. When topographical features are moderate, their impact may be masked by wind structures. Isolated patches of tall vegetation impact snow height over several tens of meters beyond their development, reducing the computed correlation, while leading to highly increased snow height.

4. Discussion and conclusions

We studied two widely different sites in terms of vegetation height, topography, and snow height. The North site had protruding vegetation and mild topography, while in the South site, shrubs were completely covered by snow and the topography was rougher. This revealed that for vegetation higher than snow height, a significant correlation between snow height and vegetation height is observed: $R^2 = 0.37$ for the North site as a whole, and $R^2 = 0.64$ for a favorable transect. For vegetation lower than snow height, there is essentially no impact of vegetation height on snow height, as $R^2 = 0.04$ in the South site. In this latter case, topography is the main predictor of snow height, with $R^2 = 0.67$ between the TPI and snow height. When vegetation is taller than snow height (North site) the correlation between the TPI and snow height is reduced, $R^2 = 0.29$, because of the interference of vegetation height. However, in this case, combining the TPI and vegetation height predicts snow height well, with $R^2 = 0.59$.

The South site also featured two spruce thickets whose impacts extend far away because of wind effects, as already noted by Sturm et al. (2001) for tall Arctic shrubs, and the resulting snow accumulation over nearby zones with lower vegetation reduces the correlation. Such snow accumulation is similar to what is caused by topographic obstacles or snow fences (Tabler 1980; Vionnet et al. 2017).

A rather simple and intuitive picture emerges from this study. Well-marked topography and vegetation taller than snow height can both independently very strongly determine snow height. When snow height exceeds vegetation height, only the effect of topography will be significantly observed. When vegetation protrudes above the snow, its effect predominates over that of moderate topography. When both protruding vegetation and topography are present, combining both vegetation height and topography provides a better prediction of snow height at our site than using just one of these variables.

These novel results, however, were obtained at one site where the snow supply is probably not limited and at only one point in time. Ideally, time series over a whole snow season would shed even more light on the interactions studied and in particular at the beginning of the season, when snow height is much lower than vegetation height. Such time series have been obtained for forests in Alpine areas (Koutantou et al. 2022; Schneider et al. 2020). This has improved our understanding of both accumulation and melt processes in forests. Alpine forests are, however, much easier to access regularly than Arctic tundra, where access in winter can be problematic and where the very cold temperatures prevent the use of UAVs. Serious challenges remain before all the aspects of snow accumulation and melt can be addressed in Arctic regions with varied vegetation and complex topography. Other variables may also deserve investigation, and in particular the snow supply. Sites with limited snow supply because of reduced areas with erodible snow, for example because of extensive shrub or tree cover (Essery and Pomeroy 2004), may show correlations different to those observed here.

Regarding ground temperature, this variable is affected by snow height because of the thermal insulation of snow. Several studies have linked variations in ground temperature to vegetation height (Grünberg et al. 2020; Kropp et al. 2021; Myers-Smith and Hik 2013; Sturm et al. 2001). Our data suggest that in areas with snow higher than vegetation such as our South site, topography may be a more important factor in determining ground temperature than vegetation height, with warmer ground temperature in hollows. However, further measurements targeting this suggestion are required to confirm it. Detailed modeling studies of snow redistribution by wind that account for both topography and vegetation (Marsh et al. 2020; Winstral et al. 2013) may both test and be tested by our conclusion, if performed at sufficiently high spatial resolution, around 1 m.

Acknowledgments. This work was funded by the Natural Sciences and Engineering Research Council of Canada (NSERC discovery grant to FD), the BNP-Paribas Foundation (APT project) and the French Polar Institute (IPEV Grant 1042). We thank the community of Umiujaq for hosting us during this study and the Centre d'Études Nordiques for the use of their facilities. Author contributions: FD designed research and obtained funding; MP coordinated the lidar data collection and initial treatment; ML, FD, JR, and GP organized data analysis and ML performed the detailed data analysis; FD and ML wrote the paper with input from JR, MP, and GP; and LA and GP advised on the research and commented on the paper. The authors declare that they have no conflict of interest.

Data availability statement. Digital terrain and surface models are available as TIFF files on the PANGAEA repository (Lamare et al. 2022). The codes used for the analysis are at https://github.com/maximlamare/umiujaq. Meteorological data since 2012 except wind direction are reported in Lackner et al. (2022). Wind direction at 10-m height is available at https://nordicana.cen.ulaval.ca/dpage.aspx?doi=45120SL-067305A53E914AF0. Topographic maps of Canada with 20-m contour lines are available at https://atlas.gc.ca/toporama/en/index.html.

REFERENCES

Barrere, M., F. Domine, M. Belke-Brea, and D. Sarrazin, 2018: Snowmelt events in autumn can reduce or cancel the soil warming effect of snow–vegetation interactions in the Arctic. *J. Climate*, **31**, 9507–9518, https://doi.org/10.1175/JCLI-D-18-0135.1.

Beck, I., R. Ludwig, M. Bernier, E. Levesque, and J. Boike, 2015: Assessing permafrost degradation and land cover changes (1986–2009) using remote sensing data over Umiujaq, sub-Arctic Quebec. *Permafrost Periglacial Process.*, **26**, 129–141, https://doi.org/10.1002/ppp.1839.

Belke-Brea, M., F. Domine, M. Barrere, G. Picard, and L. Arnaud, 2020: Impact of shrubs on winter surface albedo and snow specific surface area at a low Arctic site: In situ measurements and simulations. *J. Climate*, **33**, 597–609, https://doi.org/10.1175/JCLI-D-19-0318.1.

Boike, J., and Coauthors, 2018: A 20-year record (1998–2017) of permafrost, active layer and meteorological conditions at a high Arctic permafrost research site (Bayelva, Spitsbergen). *Earth Syst. Sci. Data*, **10**, 355–390, https://doi.org/10.5194/essd-10-355-2018.

Busseau, B.-C., A. Royer, A. Roy, A. Langlois, and F. Domine, 2017: Analysis of snow-vegetation interactions in the low Arctic-subarctic transition zone (northeastern Canada). *Phys. Geogr.*, **38**, 159–175, https://doi.org/10.1080/02723646.2017.1283477.

Costard, F., L. Dupeyrat, A. Séjourné, F. Bouchard, A. Fedorov, and B. Saint-Bézar, 2021: Retrogressive thaw slumps on ice-rich permafrost under degradation: Results from a large-scale laboratory simulation. *Geophys. Res. Lett.*, **48**, e2020GL091070, https://doi.org/10.1029/2020GL091070.

Currier, W. R., and J. D. Lundquist, 2018: Snow depth variability at the forest edge in multiple climates in the western United States. *Water Resour. Res.*, **54**, 8756–8773, https://doi.org/10.1029/2018WR022553.

——, and Coauthors, 2019: Comparing aerial lidar observations with terrestrial lidar and snow-probe transects from NASA's 2017 SnowEx campaign. *Water Resour. Res.*, **55**, 6285–6294, https://doi.org/10.1029/2018WR024533.

De Michele, C., and Coauthors, 2016: Using a fixed-wing UAS to map snow depth distribution: An evaluation at peak accumulation. *Cryosphere*, **10**, 511–522, https://doi.org/10.5194/tc-10-511-2016.

De Reu, J., and Coauthors, 2013: Application of the topographic position index to heterogeneous landscapes. *Geomorphology*, **186**, 39–49, https://doi.org/10.1016/j.geomorph.2012.12.015.

Deems, J. S., T. H. Painter, and D. C. Finnegan, 2013: Lidar measurement of snow depth: A review. *J. Glaciol.*, **59**, 467–479, https://doi.org/10.3189/2013JoG12J154.

Domine, F., M. Barrere, D. Sarrazin, S. Morin, and L. Arnaud, 2015: Automatic monitoring of the effective thermal conductivity of snow in a low-Arctic shrub tundra. *Cryosphere*, **9**, 1265–1276, https://doi.org/10.5194/tc-9-1265-2015.

——, ——, and S. Morin, 2016: The growth of shrubs on high Arctic tundra at Bylot island: Impact on snow physical properties and permafrost thermal regime. *Biogeosciences*, **13**, 6471–6486, https://doi.org/10.5194/bg-13-6471-2016

——, K. Fourteau, G. Picard, G. Lackner, D. Sarrazin, and M. Poirier, 2022: Permafrost cooled in winter by thermal bridging through snow-covered shrub branches. *Nat. Geosci.*, **15**, 554–560, https://doi.org/10.1038/s41561-022-00979-2.

Duguay, Y., and M. Bernier, 2012: The use of RADARSAT-2 and TerraSAR-X data for the evaluation of snow characteristics in subarctic regions. *2012 IEEE Int. Geoscience and Remote Sensing Symp.*, Munich, Germany, IEEE, 3556–3559, https://doi.org/10.1109/IGARSS.2012.6350650.

Essery, R., and J. Pomeroy, 2004: Vegetation and topographic control of wind-blown snow distributions in distributed and aggregated simulations for an Arctic tundra basin. *J. Hydrometeor.*, **5**, 735–744, https://doi.org/10.1175/1525-7541(2004)005<0735:VATCOW>2.0.CO;2.

Farquharson, L. M., V. E. Romanovsky, W. L. Cable, D. A. Walker, S. V. Kokelj, and D. Nicolsky, 2019: Climate change drives widespread and rapid thermokarst development in very cold permafrost in the Canadian high Arctic. *Geophys. Res. Lett.*, **46**, 6681–6689, https://doi.org/10.1029/2019GL082187.

Fernandes, R., C. Prevost, F. Canisius, S. G. Leblanc, M. Maloley, S. Oakes, K. Holman, and A. Knudby, 2018: Monitoring snow depth change across a range of landscapes with ephemeral snowpacks using structure from motion applied to lightweight unmanned aerial vehicle videos. *Cryosphere*, **12**, 3535–3550, https://doi.org/10.5194/tc-12-3535-2018.

Fortier, R., D.-R. Banville, R. Lévesque, J.-M. Lemieux, J. Molson, R. Therrien, and M. Ouellet, 2020: Development of a three-dimensional geological model, based on Quaternary chronology, geological mapping, and geophysical investigation, of a watershed in the discontinuous permafrost zone near Umiujaq (Nunavik, Canada). *Hydrogeol. J.*, **28**, 813–832, https://doi.org/10.1007/s10040-020-02113-1.

Gagnon, M., F. Domine, and S. Boudreau, 2019: The carbon sink due to shrub growth on Arctic tundra: A case study in a carbon-poor soil in eastern Canada. *Environ. Res. Commun.*, **1**, 091001, https://doi.org/10.1088/2515-7620/ab3cdd.

Grünberg, I., E. J. Wilcox, S. Zwieback, P. Marsh, and J. Boike, 2020: Linking tundra vegetation, snow, soil temperature, and permafrost. *Biogeosciences*, **17**, 4261–4279, https://doi.org/10.5194/bg-17-4261-2020.

Harder, P., M. Schirmer, J. Pomeroy, and W. Helgason, 2016: Accuracy of snow depth estimation in mountain and prairie environments by an unmanned aerial vehicle. *Cryosphere*, **10**, 2559–2571, https://doi.org/10.5194/tc-10-2559-2016.

——, J. W. Pomeroy, and W. D. Helgason, 2020: Improving sub-canopy snow depth mapping with unmanned aerial vehicles: Lidar versus structure-from-motion techniques. *Cryosphere*, **14**, 1919–1935, https://doi.org/10.5194/tc-14-1919-2020.

Jacobs, J. M., A. G. Hunsaker, F. B. Sullivan, M. Palace, E. A. Burakowski, C. Herrick, and E. Cho, 2021: Snow depth mapping with unpiloted aerial system lidar observations: A case study in Durham, New Hampshire, United States. *Cryosphere*, **15**, 1485–1500, https://doi.org/10.5194/tc-15-1485-2021.

Ju, J., and J. G. Masek, 2016: The vegetation greenness trend in Canada and US Alaska from 1984–2012 Landsat data. *Remote Sens. Environ.*, **176**, 1–16, https://doi.org/10.1016/j.rse.2016.01.001.

Koutantou, K., G. Mazzotti, and P. Brunner, 2021: UAV-based lidar high-resolution snow depth mapping in the Swiss Alps: Comparing flat and steep forests. *Int. Arch. Photogramm. Remote Sens. Spatial Inf. Sci.*, **XLIII-B3-2021**, 477–484, https://doi.org/10.5194/isprs-archives-XLIII-B3-2021-477-2021.

——, ——, ——, C. Webster, and T. Jonas, 2022: Exploring snow distribution dynamics in steep forested slopes with UAV-borne LiDAR. *Cold Reg. Sci. Technol.*, **200**, 103587, https://doi.org/10.1016/j.coldregions.2022.103587.

Kropp, H., and Coauthors, 2021: Shallow soils are warmer under trees and tall shrubs across Arctic and boreal ecosystems. *Environ. Res. Lett.*, **16**, 015001, https://doi.org/10.1088/1748-9326/abc994.

Lackner, G., F. Domine, D. Sarrazin, D. Nadeau, and M. Belke-Brea, 2022: Hydrometeorological, snow and soil data from a low-Arctic valley in the forest-tundra ecotone in Northern Quebec.

PANGAEA, accessed 13 April 2023, https://doi.org/10.1594/PANGAEA.946538.

Lamare, M., F. Domine, J. Revuelto, M. Pelletier, L. Arnaud, and G. Picard, 2022: UAV-borne lidar campaign over Umiuaq, Hudson Bay, Canada in 2017 and 2018. PANGAEA, accessed 13 April 2023, https://doi.org/10.1594/PANGAEA.943854.

Lemay, M.-A., L. Provencher-Nolet, M. Bernier, E. Lévesque, and S. Boudreau, 2018: Spatially explicit modeling and prediction of shrub cover increase near Umiujaq, Nunavik. *Ecol. Monogr.*, **88**, 385–407, https://doi.org/10.1002/ecm.1296.

Liston, G. E., J. P. McFadden, M. Sturm, and R. A. Pielke, 2002: Modelled changes in Arctic tundra snow, energy and moisture fluxes due to increased shrubs. *Global Change Biol.*, **8**, 17–32, https://doi.org/10.1046/j.1354-1013.2001.00416.x.

Marsh, C. B., J. W. Pomeroy, R. J. Spiteri, and H. S. Wheater, 2020: A finite volume blowing snow model for use with variable resolution meshes. *Water Resour. Res.*, **56**, e2019WR025307, https://doi.org/10.1029/2019WR025307.

Mazzotti, G., W. R. Currier, J. S. Deems, J. M. Pflug, J. D. Lundquist, and T. Jonas, 2019: Revisiting snow cover variability and canopy structure within forest stands: Insights from airborne lidar data. *Water Resour. Res.*, **55**, 6198–6216, https://doi.org/10.1029/2019WR024898.

McGuire, A. D., and Coauthors, 2018: Dependence of the evolution of carbon dynamics in the northern permafrost region on the trajectory of climate change. *Proc. Natl. Acad. Sci. USA*, **115**, 3882–3887, https://doi.org/10.1073/pnas.1719903115.

Mithan, H. T., T. C. Hales, and P. J. Cleall, 2021: Topographic and ground-ice controls on shallow landsliding in thawing Arctic permafrost. *Geophys. Res. Lett.*, **48**, e2020GL092264, https://doi.org/10.1029/2020GL092264.

Myers-Smith, I. H., and D. S. Hik, 2013: Shrub canopies influence soil temperatures but not nutrient dynamics: An experimental test of tundra snow-shrub interactions. *Ecol. Evol.*, **3**, 3683–3700, https://doi.org/10.1002/ece3.710.

Painter, T. H., and Coauthors, 2016: The airborne snow observatory: Fusion of scanning lidar, imaging spectrometer, and physically-based modeling for mapping snow water equivalent and snow albedo. *Remote Sens. Environ.*, **184**, 139–152, https://doi.org/10.1016/j.rse.2016.06.018.

Pelletier, M., M. Allard, and E. Lévesque, 2019: Ecosystem changes across a gradient of permafrost degradation in subarctic Québec (Tasiapik Valley, Nunavik, Canada). *Arctic Sci.*, **5** (1), 1–26, https://doi.org/10.1139/as-2016-0049.

Pomeroy, J. W., D. M. Gray, and P. G. Landine, 1993: The prairie blowing snow model: Characteristics, validation, operation. *J. Hydrol.*, **144**, 165–192, https://doi.org/10.1016/0022-1694(93)90171-5.

Proulx, H., J. M. Jacobs, E. A. Burakowski, E. Cho, A. G. Hunsaker, F. B. Sullivan, M. Palace, and C. Wagner, 2022: Comparison of in-situ snow depth measurements and impacts on validation of unpiloted aerial system Lidar over a mixed-use temperate forest landscape. *Cryosphere Discuss.*, https://doi.org/10.5194/tc-2022-7.

Provencher-Nolet, L., M. Bernier, and E. Levesque, 2014: Quantification of recent changes to the forest- tundra ecotone through numerical analysis of aerial photographs. *Ecoscience*, **21**, 419–433, https://doi.org/10.2980/21-(3-4)-3715.

Revuelto, J., J. I. López-Moreno, C. Azorin-Molina, J. Zabalza, G. Arguedas, and S. M. Vicente-Serrano, 2014: Mapping the annual evolution of snow depth in a small catchment in the Pyrenees using the long-range terrestrial laser scanning. *J. Maps*, **10**, 379–393, https://doi.org/10.1080/17445647.2013.869268.

——, P. Billecocq, F. Tuzet, B. Cluzet, M. Lamare, F. Larue, and M. Dumont, 2020: Random forests as a tool to understand the snow depth distribution and its evolution in mountain areas. *Hydrol. Processes*, **34**, 5384–5401, https://doi.org/10.1002/hyp.13951.

——, J. I. López-Moreno, and E. Alonso-González, 2021: Light and shadow in mapping alpine snowpack with unmanned aerial vehicles in the absence of ground control points. *Water Resour. Res.*, **57**, e2020WR028980, https://doi.org/10.1029/2020WR028980.

Salinas-Melgoza, M. A., M. Skutsch, and J. C. Lovett, 2018: Predicting aboveground forest biomass with topographic variables in human-impacted tropical dry forest landscapes. *Ecosphere*, **9**, e02063, https://doi.org/10.1002/ecs2.2063.

Schneider, D., N. P. Molotch, J. S. Deems, and T. H. Painter, 2020: Analysis of topographic controls on depletion curves derived from airborne lidar snow depth data. *Hydrol. Res.*, **52**, 253–265, https://doi.org/10.2166/nh.2020.267.

Sturm, M., J. Holmgren, and G. E. Liston, 1995: A seasonal snow cover classification-system for local to global applications. *J. Climate*, **8**, 1261–1283, https://doi.org/10.1175/1520-0442(1995)008<1261:ASSCCS>2.0.CO;2.

——, J. P. McFadden, G. E. Liston, F. S. Chapin III, C. H. Racine, and J. Holmgren, 2001: Snow-shrub interactions in Arctic tundra: A hypothesis with climatic implications. *J. Climate*, **14**, 336–344, https://doi.org/10.1175/1520-0442(2001)014<0336:SSIIAT>2.0.CO;2.

——, T. Douglas, C. Racine, and G. E. Liston, 2005a: Changing snow and shrub conditions affect albedo with global implications. *J. Geophys. Res.*, **110**, G01004, https://doi.org/10.1029/2005JG000013.

——, J. Schimel, G. Michaelson, J. M. Welker, S. F. Oberbauer, G. E. Liston, J. Fahnestock, and V. E. Romanovsky, 2005b: Winter biological processes could help convert Arctic tundra to shrubland. *BioScience*, **55**, 17–26, https://doi.org/10.1641/0006-3568(2005)055[0017:WBPCHC]2.0.CO;2.

Tabler, R. D., 1980: Geometry and density of drifts formed by snow fences. *J. Glaciol.*, **26**, 405–419, https://doi.org/10.1017/S0022143000010935.

Tinkham, W. T., A. M. S. Smith, H.-P. Marshall, T. E. Link, M. J. Falkowski, and A. H. Winstral, 2014: Quantifying spatial distribution of snow depth errors from LiDAR using random forest. *Remote Sens. Environ.*, **141**, 105–115, https://doi.org/10.1016/j.rse.2013.10.021.

Tremblay, B., E. Levesque, and S. Boudreau, 2012: Recent expansion of erect shrubs in the low Arctic: Evidence from eastern Nunavik. *Environ. Res. Lett.*, **7**, 035501, https://doi.org/10.1088/1748-9326/7/3/035501.

Uhlmann, Z., N. F. Glenn, L. P. Spaete, C. Hiemstra, C. Tennant, and J. McNamara, 2018: Resolving the influence of forest-canopy structure on snow depth distributions with terrestrial laser scanning. *2018 IEEE Int. Geoscience and Remote Sensing Symp.*, Valencia, Spain, IEEE, 6284–6286, https://doi.org/10.1109/IGARSS.2018.8517911.

Vionnet, V., E. Martin, V. Masson, C. Lac, F. N. Bouvet, and G. Guyomarc'h, 2017: High-resolution large eddy simulation

of snow accumulation in alpine terrain. *J. Geophys. Res. Atmos.*, **122**, 11 005–11 021, https://doi.org/10.1002/2017JD026947.

Winstral, A., and D. Marks, 2002: Simulating wind fields and snow redistribution using terrain-based parameters to model snow accumulation and melt over a semi-arid mountain catchment. *Hydrol. Processes*, **16**, 3585–3603, https://doi.org/10.1002/hyp.1238.

——, ——, and R. Gurney, 2013: Simulating wind-affected snow accumulations at catchment to basin scales. *Adv. Water Resour.*, **55**, 64–79, https://doi.org/10.1016/j.advwatres.2012.08.011.

Zhang, T., 2005: Influence of the seasonal snow cover on the ground thermal regime: An overview. *Rev. Geophys.*, **43**, RG4002, https://doi.org/10.1029/2004RG000157.